Pergamon

PII: S0045-7930(96)00039-4

Computers & Fluids Vol. 26, No. 3, pp. 233–247, 1997

0045-7930/97 $17.00 + 0.00

A SECOND-ORDER SPACE AND TIME NODAL METHOD FOR THE ONE-DIMENSIONAL CONVECTION–DIFFUSION EQUATION

RIZWAN-UDDIN*

Department of Mechanical, Aerospace and Nuclear Engineering, University of Virginia, Thornton Hall, Charlottesville, VA 22903-2442, U.S.A.

(Received 8 April 1996; in revised form 29 July 1996)

Abstract—We present a nodal integral method for the one-dimensional convection–diffusion equation. The development is carried out in the nodal spirit, and results in a method that is second order both in space and time variables. Extension of this method, which is characterized by inherent upwinding, to multi-dimensional problems is straightforward. The nodal method's ability to yield accurate results on rather coarse mesh sizes when coupled with node interior reconstruction of the solution results in a rather powerful scheme that can accurately resolve the solution—even in regions with sharp gradients—with relatively large node sizes. Three widely used problems are solved numerically to demonstrate the properties of the nodal method developed here. © 1997 Elsevier Science Ltd. All rights reserved.

1. INTRODUCTION

Accurate solution of the time-dependent convection–diffusion equation on large spatial domains and for large times is desirable. This requires the development of numerical schemes that can remain accurate even for large node sizes and large time steps. Several effective schemes have been proposed to achieve this goal [1]. Each has its own advantages and disadvantages. More recently, the operator splitting schemes have become popular [2–6]. The disadvantage with the operator splitting method is that the boundary conditions are available for the actual operator, and not for the split-operators. To resolve the issue of boundary conditions, several schemes have been suggested to determine the boundary conditions for the split operators, and significant improvement in numerical accuracy and efficiency has been gained [7–9].

Numerical schemes that have been successfully applied to other problems [10–18] are also being developed to solve the convection–diffusion equation. In this paper we present a scheme that in recent years has been successfully applied to several problems, including the Burgers equation [18, 19], Navier–Stokes equation [14, 18], etc. Among the so-called coarse-mesh nodal methods that have been developed over the last two decades, the nodal integral method (NIM) has probably been applied to more problems than any other method. NIM and the nodal greens tensor method (NGTM) [10] have been shown both formally and numerically to be equivalent [12]. The advantage of NIM over NGTM is that the former is simpler in formulation and leads to fewer unknowns per node. NIM's past applications to the convection–diffusion equation were restricted to a two-dimensional, steady-state convection–diffusion equation [16, 17], and to a general three-dimensional time-dependent convection–diffusion equation in which the time variable was treated using the finite-difference approach [15] (rather than the nodal approach used for the space coordinate).

A recent extension of the conventional nodal integral method—actually motivated by the successful applications to the two-dimensional steady-state convection–diffusion equation that resulted in inherent upwinding in the final scheme—to nonlinear problems has successfully introduced inherent upwinding even in nonlinear problems, such as the Burgers equation [19].

We present here the development of a NIM for the one-dimensional time-dependent convection–diffusion equation in which both space, and time coordinates have been treated in the spirit of the nodal method. Our present development is second order in both space and time. Before

*Current address: Department of Nuclear Engineering and Computational Science and Engineering, University of Illinois, Urbana, IL 61801, U.S.A.

we present the development of the NIM for the time-dependent convection–diffusion equation, we would like to point out that second and third-order NIM have been developed for the two-dimensional steady-state convection–diffusion equation [16, 17]. Although the general multi-dimensional time-dependent convection–diffusion equation has been solved using the nodal integral method [15], the nodal approach was employed in that work only for the spatial variables, while the time variable was treated using the finite-difference approach. The development reported here is nodal in both space and time. Hence, the method reported here reduces to those reported earlier for the steady-state convection–diffusion equation.

2. FORMALISM

The method described here is similar to the modified nodal integral method recently proposed for the nonlinear PDEs in the context of Burgers equation [19]. Since the flow field for the linear convection–diffusion equation is explicitly known, the approximation introduced for the Burgers equation—where the velocity $u(x,t)$ in the nonlinear term $(u(x,t)\,\partial u(x,t)/(\partial x))$ was assumed constant over the node—is not needed. Instead, for the convection–diffusion equation, exact node-averaged velocities are used when treating the convection term.

The one-dimensional time-dependent convection–diffusion equation for concentration $C(x,t)$ is

$$\frac{\partial C(x,t)}{\partial t} + u\frac{\partial C(x,t)}{\partial x} - \frac{1}{R}\frac{\partial^2 C(x,t)}{\partial x^2} = 0 \tag{1}$$

where R is the reciprocal of the diffusion coefficient, D. Dividing the computational domain into n_x spatial nodes, where each node is of width $2a_i$, we define a local coordinate system in each space–time node with the origin at node center. Nodes in the spatial direction are indexed with subscript i. Time is indexed with subscript j, and the solution will be determined at time intervals of 2τ. The nodalization scheme is shown in Fig. 1, where each space–time node is of width $2a_{ij}$ and height 2τ. The discrete variables associated with each node (i,j) will be the space-averaged (over the node width) concentration at time t, $\bar{C}^x_{ij}$, and the time-averaged (over the time step) concentration at x, $\bar{C}^t_{ij}$ where

$$\bar{C}^x_{ij}(t) \equiv \frac{1}{(2a_{ij})}\int_{-a_{ij}}^{+a_{ij}} C(x,t)\,\mathrm{d}x \tag{2}$$

$$\bar{C}^t_{ij}(x) \equiv \frac{1}{(2\tau)}\int_{-\tau}^{+\tau} C(x,t)\,\mathrm{d}t\,. \tag{3}$$

Operating equation (1) with $1/2\tau\int_{-\tau}^{+\tau}\mathrm{d}t$,we get the time-averaged space-dependent convection–diffusion equation

$$\frac{1}{R}\frac{\mathrm{d}^2\bar{C}^t(x)}{\mathrm{d}x^2} - u\frac{\mathrm{d}\bar{C}^t(x)}{\mathrm{d}x} = \bar{S}^t_2(x) \equiv \frac{1}{(2\tau)}\int_{-\tau}^{\tau}\frac{\partial C(x,t)}{\partial t}\,\mathrm{d}t \tag{4}$$

and operating equation (1) with $1/2a_i\int_{-a_i}^{+a_i}\mathrm{d}x$, we get the space-averaged time-dependent convection–diffusion equation

$$\frac{\mathrm{d}\bar{C}^x(t)}{\mathrm{d}t} = \bar{S}^x_1(t) \equiv \frac{1}{(2a_{ij})}\int_{-a_{ij}}^{+a_{ij}}\left[\frac{1}{R}\frac{\partial^2 C(x,t)}{\partial x^2} - u\frac{\partial C(x,t)}{\partial x}\right]\mathrm{d}x\,. \tag{5}$$

To be precise, transverse averaged quantities in equations (4) and (5) must have subscripts (i,j), as these are local integrations over individual nodes. The subscripts are dropped here for convenience. Solutions of equations (4) and (5) yield the time-averaged and space-averaged solutions for the concentration $C(x,t)$. In the spirit of the nodal integral method, equations (4) and (5) must be solved analytically, keeping as much of each equation as possible *involved* in determining the analytical solution. This means that those terms in each equation which make an analytical solution out of reach, must be lumped on the right-hand side in, what are called, the pseudo-source terms.

Inhomogeneous solutions are obtained by expanding these pseudo-source terms in, say, Legendre polynomials in the independent variable. The coefficients of these expansions are additional unknowns which must be evaluated. Traditionally, additional equations are obtained for these coefficients by imposing certain constraints, such as the conservation of the original PDE over each computational domain, and uniqueness of the node-averaged dependent variables.

We expand the pseudo-source term in the Legendre polynomial, truncate at the zeroth order, and solve equation (4) analytically

$$\bar{C}'(x) = \bar{C}'(-a_{i,j}) + \frac{\mathrm{d}\bar{C}_x^t(-a_{i,j})}{\mathrm{d}x}\left[\frac{e^{[Ru(x+a_{i,j})]}-1}{(Ru)}\right] + \frac{(R\bar{S}_2^{tx})}{(Ru_{i,j}^0)}\left[\frac{e^{[Ru(x+a_{i,j})]}-1}{(Ru)} - \left(x+a_{i,j}\right)\right]. \tag{6}$$

Equation (6) was obtained by assuming that the time-averaged concentration $\bar{C}'(-a_{i,j})$ and its derivative $\mathrm{d}\bar{C}'(-a_{i,j})/\mathrm{d}x$ at the *left* edge of the node are known. Another expression for

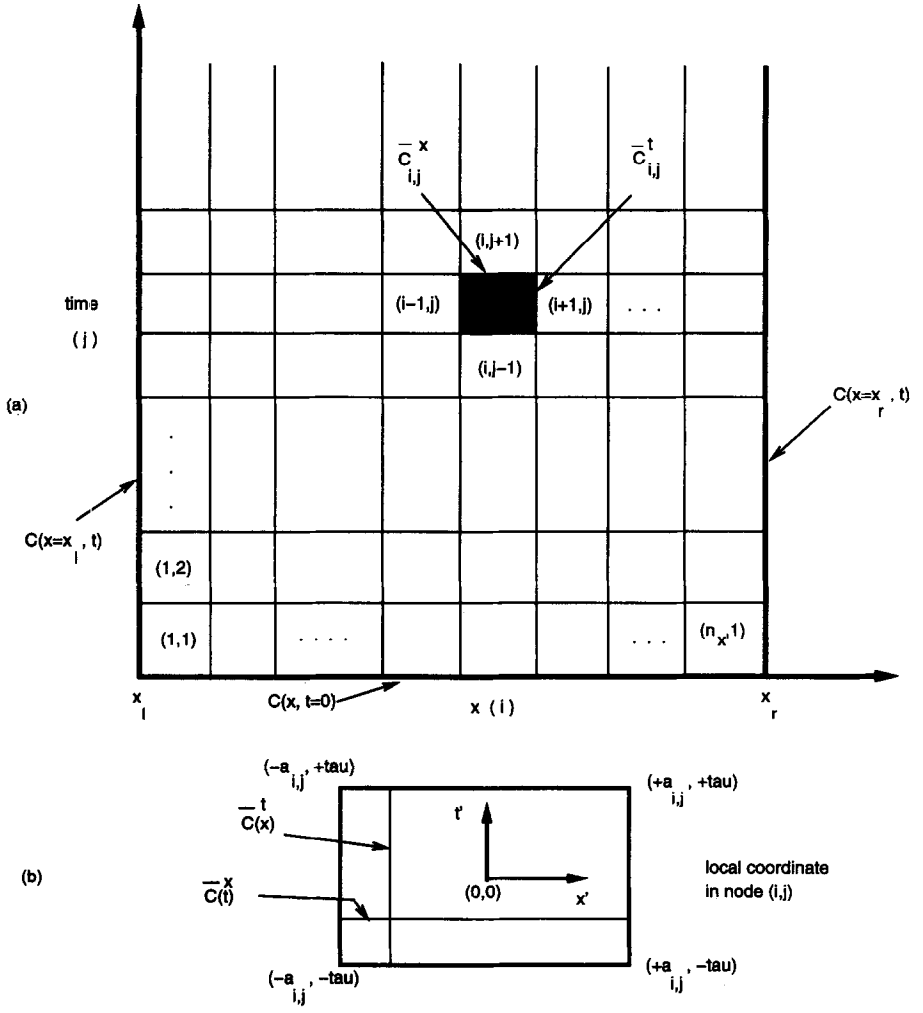

Fig. 1. (a) Schematic diagram of the global (x,t) space, and its division into computational elements or nodes. (b) Local coordinate system within the node (i,j). In the text, primes on x' and t' are dropped for convenience.

$\bar{C}^t(x)$ can be written by assuming the boundary conditions to be known on the *right* edge of the node

$$\bar{C}^t(x) = \bar{C}^t(+a_{i,j}) - \frac{d\bar{C}^t(a_{i,j})}{dx}\left[\frac{1-e^{-[Ru(a_{i,j}-x)]}}{(Ru)}\right] - \frac{(R\bar{S}_2^{tx})}{(Ru)}\left\{\frac{[1-e^{-Ru(a_{i,j}-x)}]}{(Ru)} - (a_{i,j}-x)\right\}. \tag{7}$$

We now want to equate the derivative on the two sides of an interface (between node (i,j) and node $(i+1,j)$). Letting $i \to i+1$ in equation (6), evaluating it at $x = +a_{i+1,j}$, we solve for the derivative on the right side of the interface, $d\bar{C}^t_{i+1,j}(-a_{i+1,j})/dx$. The derivative on the left side can be determined directly from equation (7), by simply evaluating it at $x = -a_{i,j}$ and solving for $d\bar{C}^t_{i,j}(a_{i,j})/dx$. Equating the two derivatives and realizing that $\bar{C}^t_{i,j}(+a_{i,j}) = \bar{C}^t_{i+1,j}(-a_{i+1,j})$, we obtain the three-point scheme that relates $\bar{C}^t_{i-1,j}$, $\bar{C}^t_{i,j}$ and $\bar{C}^t_{i+1,j}$

$$\left\{\frac{Ru}{[1-e^{-2Rua_{i,j}}]}\right\}\bar{C}^t_{i-1,j} - \left\{\frac{Ru}{[1-e^{-2Rua_{i,j}}]} + \frac{Ru}{[e^{2Rua_{i+1,j}}-1]}\right\}\bar{C}^t_{i,j} + \left\{\frac{Ru}{[e^{2Rua_{i+1,j}}-1]}\right\}\bar{C}^t_{i+1,j}$$
$$= R\bar{S}^{tx}_{2,(i,j)}\left\{\frac{2a_{i,j}}{[1-e^{-2Rua_{i,j}}]} - \frac{1}{Ru}\right\} + R\bar{S}^{tx}_{2,(i+1,j)}\left\{\frac{1}{Ru} - \frac{2a_{i+1,j}}{[e^{2Rua_{i+1,j}}-1]}\right\} \tag{8}$$

where time-averaged concentration in each node is understood to be evaluated at the right spatial (node) boundary ($\bar{C}^t_{i,j} \equiv \bar{C}^t_{i,j}(x = +a_{i,j})$). The requirement of the continuity of concentration and its derivative on node interfaces is physical. It ensures that the convected and diffused mass flowing into a node boundary (over a time step Δt) is the same as that which comes out on the other side. Requiring continuity of the derivative ensures that (assuming the same diffusion coefficients in neighboring nodes) the method, even in the limit of small Pe, is conservative. For very large Pe, the continuity of the derivative condition can possibly be relaxed to allow better resolution of steep fronts.

The solution of equation (5) for $\bar{C}^x(t)$ is straightforward. The linear node interior solution—obtained after expanding the source term $\bar{S}^x_1(t)$ in Legendre polynomial and truncating at the zeroth order—is given by

$$\bar{C}^x(t) = \bar{C}^x(-\tau) + \bar{S}^{xt}_1(\tau + t) \tag{9}$$

which, when evaluated at $t = +\tau$, becomes

$$\bar{C}^x(\tau) = \bar{C}^x(-\tau) + 2\tau\bar{S}^{xt}_1. \tag{10}$$

Equation (10) written in terms of subscripts (i,j) is

$$\bar{C}^x_{i,j} = \bar{C}^x_{i,j-1} + 2\tau\bar{S}^{xt}_{1,(i,j)}. \tag{11}$$

With equations (8) and (11) for each node, we have two equations but four unknowns per node ($\bar{C}^x_{i,j}$, $\bar{C}^t_{i,j}$, $\bar{S}^{xt}_{1,(i,j)}$, $\bar{S}^{tx}_{2,(i,j)}$). The other two equations per node are obtained from physical constraints. Simply integrating the original convection–diffusion equation over the (space–time) node (i,j)

$$\frac{1}{4a_{i,j}\tau}\int_{-a_{i,j}}^{+a_{i,j}}\int_{-\tau}^{+\tau}[\text{equation (1)}]\,d\tau dx \tag{12}$$

yields the first constraint equation. Realizing the definitions of $\bar{S}^{xt}_{1,(i,j)}$ and $\bar{S}^{tx}_{2,(i,j)}$ (equations (4) and (5)), the above equation becomes

$$\bar{S}^{xt}_{1,(i,j)} = \bar{S}^{tx}_{2,(i,j)}. \tag{13}$$

The second constraint equation is obtained by equating $\bar{C}^{xt}_{(i,j)}$ and $\bar{C}^{tx}_{(i,j)}$. Operating equation (6) with $1/2\tau \int_{-\tau}^{\tau} dt$ yields an expression for $\bar{C}^{xt}_{(i,j)}$, and operating equation (9) with $1/2a_{i,j} \int_{-a_{i,j}}^{+a_{i,j}} dx$ yields an expression for $\bar{C}^{tx}_{(i,j)}$. Equating the two, results in the last of the four equations

$$\bar{C}^{x}_{i,j-1} + \tau \bar{S}^{xt}_{1,(i,j)} = \left\{ \frac{1}{2Rua_{i,j}} - \frac{1}{[e^{2Rua_{i,j}} - 1]} \right\} \bar{C}^{t}_{i,j} + \left\{ 1 - \frac{1}{2Rua_{i,j}} + \frac{1}{[e^{2Rua_{i,j}} - 1]} \right\} \bar{C}^{t}_{i-1,j} + (R\bar{S}^{tx}_{2,(i,j)}) \left\{ \frac{1}{(Ru)^2} - \frac{a_{i,j}}{(Ru)} - \frac{2a_{i,j}}{(Ru)[e^{2Rua_{i,j}} - 1]} \right\}. \quad (14)$$

From the set of four equations ((8), (11), (13) and (14)) for the four unknowns per node ($\bar{C}^{x}_{i,j}$, $\bar{C}^{t}_{i,j}$, $\bar{S}^{xt}_{1,(i,j)}$, $\bar{S}^{tx}_{2,(i,j)}$), we eliminate the node-averaged pseudo-source terms $\bar{S}^{xt}_{1,(i,j)}$ and $\bar{S}^{tx}_{2,(i,j)}$, and obtain the following two equations for $\bar{C}^{t}_{(i,j)}$ and $\bar{C}^{x}_{(i,j)}$:

$$\left(\frac{X_{i,j} - \tau}{\tau} \right) \bar{C}^{x}_{i,j} - \left(\frac{X_{i,j} + \tau}{\tau} \right) \bar{C}^{x}_{i,j-1} + 2A_{i,j} \bar{C}^{t}_{i,j} + 2B_{i,j} \bar{C}^{t}_{i-1,j} = 0 \quad (15)$$

where

$$D_{i,j} \bar{C}^{t}_{i-1,j} + E_{i,j} \bar{C}^{t}_{i,j} + F_{i+1,j} \bar{C}^{t}_{i+1,j} = \left(\frac{\bar{C}^{x}_{i,j} + \bar{C}^{x}_{i,j-1}}{2(X_{i,j}/R)} \right) G_{i,j} + \left(\frac{\bar{C}^{x}_{i+1,j} + \bar{C}^{x}_{i+1,j-1}}{2(X_{i+1,j}/R)} \right) 2a_{i+1,j} A_{i+1,j} \quad (16)$$

$$A_{i,j} \equiv \left\{ \frac{1}{2a_{i,j} Ru} - H_{i,j} \right\}$$

$$B_{i,j} \equiv 1 - A_{i,j}$$

$$\frac{X_{i,j}}{R} \equiv \left\{ \frac{1}{(Ru)^2} - \frac{a_{i,j}}{(Ru)} - \frac{2a_{i,j} H_{i,j}}{(Ru)} \right\}$$

$$D_{i,j} \equiv RuI_{i,j} + \frac{(1 - A_{i,j})}{(X_{i,j}/R)} G_{i,j}$$

$$E_{i,j} \equiv \frac{A_{i,j} G_{i,j}}{(X_{i,j}/R)} + \frac{2a_{i+1,j} A_{i+1,j} (1 - A_{i+1,j})}{(X_{i+1,j}/R)} - RuI_{i,j} - RuH_{i+1,j}$$

$$F_{i,j} \equiv (Ru) H_{i,j} + \frac{2A^2_{i,j} a_{i,j}}{(X_{i,j}/R)}$$

$$G_{i,j} \equiv 2a_{i,j} I_{i,j} - \frac{1}{(Ru)}$$

$$H_{i,j} \equiv \frac{1}{[e^{2a_{i,j} Ru} - 1]}$$

$$I_{i,j} \equiv \frac{1}{[1 - e^{-2a_{i,j} Ru}]}.$$

Before we apply the method developed above to benchmark problems, two features of this scheme must be pointed out. First, the method has inherent upwinding built in. The relative influence of concentration in two neighboring nodes on either side ($\bar{C}^{t}_{i-1,j}$ and $\bar{C}^{t}_{i+1,j}$) on the concentration in the node (i,j) $\bar{C}^{t}_{i,j}$, automatically depends upon the flow direction, speed and diffusion coefficient. This inherent upwinding also resulted in earlier application of the nodal integral method to the convection–diffusion equation. Second, the development presented above automatically yields expressions for node interior distribution of concentration (both $\bar{C}^{x}(t)$and $\bar{C}^{t}(x)$ are available). This characteristic of the NIM allows rather accurate reconstruction of the solution even when the

problem is solved with large node sizes. For example, an expression for $\bar{C}'(x)$ can be written by evaluating equation (6) at $x = +a_{i,j}$, solving for the derivative $d\bar{C}'(-a_{i,j})/dx$, and substituting the resulting expression back into equation (6).

3. NUMERICAL EXAMPLES

We solve three classic problems to demonstrate the properties of the method developed here. The first is the propagating front problem in which a step change in concentration is propagated forward as the front diffuses. Constant boundary conditions are imposed on the domain edges. To study the effect of time-dependent boundary conditions, a modified form of the first problem is studied in which the concentration on one of the boundaries decreases exponentially in time. The third problem is that of the propagation and diffusion of a Gaussian hump.

The nodal method presented here and those developed earlier exactly solve the one-dimensional steady-state convection–diffusion equation (the classic 'tough' problem). No matter how large the Peclet number is, the nodal integral methods yield the exact solution with a single node covering the entire domain. After all, it is this exact solution of the steady-state problem that forms the basis of the time-averaged space-dependent solution of the time-dependent problem.

One of the characteristic features of the nodal integral method is that the discrete variables are quantities averaged over node surfaces, rather than at grid points as is the case in finite-difference methods. This feature of NIM necessitates that for any quantitative error analysis, time-averaged and space-averaged exact solutions must be known. Although exact solutions are available for all three problems studied here, we evaluate the time-averaged (over a time step for fixed x) and space-averaged (over a node for fixed t) solutions only for the first problem, and use that as a reference to (numerically) carry out the error analysis of the method developed here.

3.1. Example 1

First we study the propagating concentration front problem [1]. The domain is restricted to $-2 \leq x \leq 2$. The initial and boundary conditions are

$$C(x,0) = \begin{cases} 1.0 & -2 \leq x < 0 \\ 0.0 & 0 < x \leq 2 \end{cases}$$

and

$$C(x = -2,t) = 1.0 \quad C(x = 2,t) = 0.0.$$

An exact solution is

$$C(x,t) = 0.5 - \frac{2}{\pi} \sum_{k=1}^{\infty} \frac{\sin\left[\dfrac{(2k-1)\pi(x-ut)}{L}\right] \exp\left[\dfrac{-\alpha(2k-1)^2\pi^2 t}{L^2}\right]}{(2k-1)}. \tag{17}$$

The exact solution averaged over the width of a node is

$$\bar{C}^x(t) = 0.5 - \frac{2L}{(2a)\pi^2} \sum_{k=1}^{\infty} \frac{\exp\left[\dfrac{[-\alpha(2k-1)^2\pi^2 t]}{L^2}\right]}{(2k-1)^2} \left[\cos\left[\frac{(2k-1)\pi(x_l - ut)}{L}\right] - \cos\left[\frac{(2k-1)\pi(x_r - ut)}{L}\right]\right] \tag{18}$$

where x_l and x_r are the space coordinates of the left and right boundaries of the node. Exact solution averaged over a time step of height 2τ (from $(t_f - 2\tau)$ to t_f) is

$$\bar{C}'(x) = 0.5 - \frac{2}{(2\tau)\pi} \sum_{k=1}^{\infty} \frac{1}{(2k-1)} \left\{ \frac{e^{-\beta_3 t_f}}{(\beta_3^2 + \beta_2^2)} \left[\beta_2 \cos\left(\beta_1 - \beta_2 t_f\right) - \beta_3 \sin\left(\beta_1 - \beta_2 t_f\right) \right] \right.$$
$$\left. - \frac{e^{-\beta_3 (t_f - 2\tau)}}{(\beta_3^2 + \beta_2^2)} \left[\beta_2 \cos\left(\beta_1 - \beta_2 \left(t_f - 2\tau\right)\right) - \beta_3 \sin\left(\beta_1 - \beta_2 \left(t_f - 2\tau\right)\right) \right] \right\} \quad (19)$$

where

$$\beta_1 = \frac{(2k-1)\pi x}{L} \quad \beta_2 = \frac{(2k-1)\pi u}{L} \quad \beta_3 = \frac{\alpha(2k-1)^2\pi^2}{L^2}.$$

Root mean square error is defined as

$$RMS = \frac{1}{N^{1/2}} \sqrt{\sum_{i=1}^{N} (C_i - C_{i,\text{exact}})^2}. \quad (20)$$

The exact solution and solution obtained using the method developed here are plotted in Fig. 2 for $R = 33.3$ at $t = 0.5$ and 1.0. Space-averaged values $\bar{C}^x$, are plotted in Fig. 2(a) (at the center of the corresponding nodes), and time-averaged values $\bar{C}^t$ are plotted in Fig. 2(b). Clearly, the scheme developed here can very faithfully track the propagating front. RMS errors for this case in $\bar{C}^x$, $\bar{C}^t$, and in both $\bar{C}^x$ and $\bar{C}^t$ values are 0.3687×10^{-2}, 0.2786×10^{-2} and 0.3274×10^{-2}, respectively.

To analyze the order of the method, we solve the above problem with a fine time step ($2\tau = 0.01$) for different node sizes. RMS errors are tabulated in Table 1 and plotted versus node size in Fig. 3. The slope is ~ 1.97 indicating $O(a^2)$. We next solved the problem with exact solution at $t = 0.8$ as initial condition, and fine spatial discretization ($\Delta x = 2a = 0.08$) for 10 time steps for different time increments. The initial condition is specified at $t = 0.8$ rather than at $t = 0.0$ in order for the step change in concentration to not contaminate the error analysis. RMS errors are tabulated in Table 2, and plotted versus time step size (2τ) in Fig. 4. The slope in Fig. 4 is ~ 1.88, again approximately indicating $O(\tau^2)$. As is well known, at very small time increments—when error due to spatial discretization starts to contribute significantly to the total error—the order (slope) drops below 2.

The NIM performs quite well even as the problem is made more difficult by reducing the diffusion coefficient (increasing Peclet number, convection dominated), for fixed node size. Concentration profiles at $t = 1$—with initial condition specified at $t = 0$—for different diffusion coefficients are shown in Fig. 5. Even at a cell Reynolds number ($u\Delta x/D = u\Delta x R$) of 6500, the nodal method developed here is rather accurate. It is interesting to note that the RMS errors for $R = 50$, 500 and 6500 are 0.4384×10^{-2}, 0.1945×10^{-1} and 0.1217×10^{-1}, respectively, indicating a small improvement in accuracy for highly convective problems. The steep concentration front for the $R = 6500$ case, is accurately resolved with only two nodes covering the entire width of the front. For comparison with the nodal method presented here, we choose the Crank–Nicolson, four-point upwind scheme (CN-4PU), and use the code given in Ref. [1], to evaluate the error from the CN-4PU scheme. RMS errors for the NIM and CN-4PU scheme for different values of R are tabulated in Table 3. The RMS error in the CN-4PU scheme increases as R is increased reaching an asymptotic value at about $R = 1000$. As noticed above, the RMS in NIM, on the other hand, first increases and then starts to decrease with increasing R, indicating that NIM can more accurately solve the limiting pure convection problem and the limiting pure diffusion problem than it can solve an evenly balanced convection–diffusion problem. As a result, the error in NIM—which is less than the error in the CN-4PU scheme by a factor of about two for $R = 100$—is better than

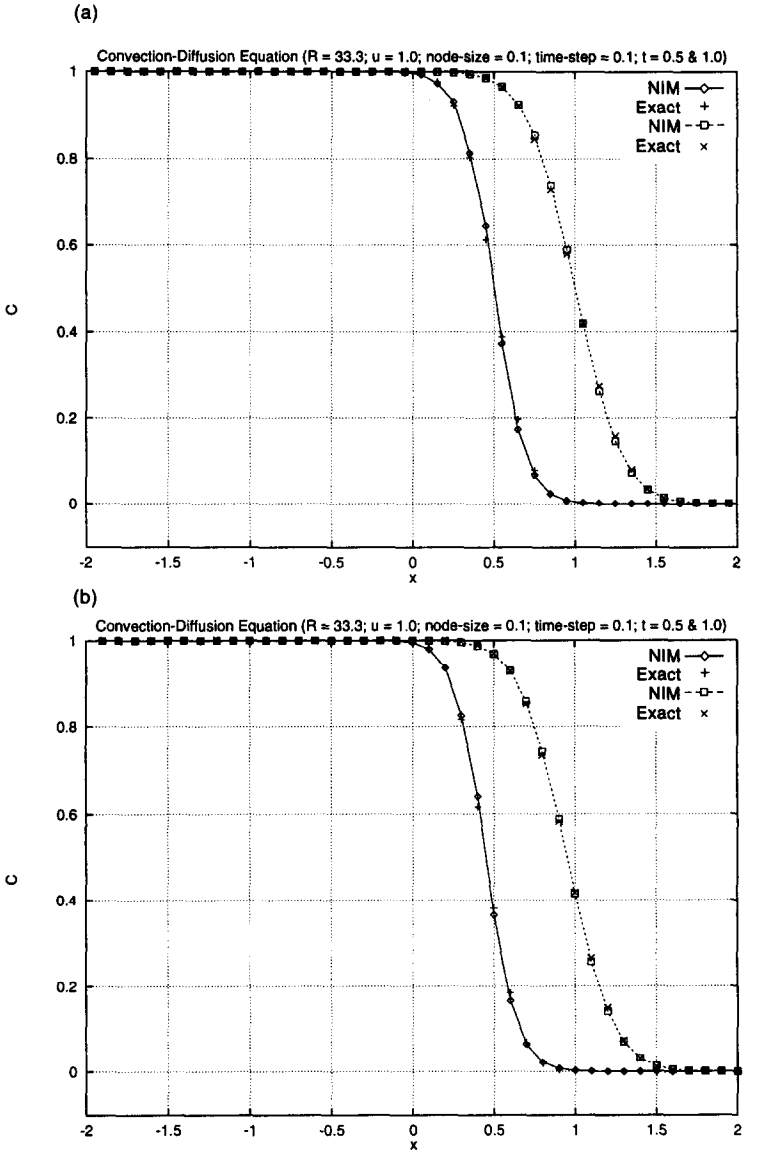

Fig. 2. A general comparison of results obtained using the NIM with exact solution: (a) space-averaged solution $\bar{C}^x$; (b) time-averaged solution $\bar{C}^t$.

the error in the CN-4PU scheme by a factor of 4.5 at $R = 6500$. For $R = 6500$, the results of NIM and the CN-4PU scheme are plotted for $0 < x < 2$ in Fig. 6. Corresponding exact solutions are also plotted. Note that the NIM solutions are the concentration averaged over the last time step (from $t = 0.9$ to 1.0), whereas the CN-4PU and its corresponding exact solution are at $t = 1.0$. As is well known, a particular choice of parameters in the CN-4PU scheme, while eliminating

Table 1. RMS error vs node size

$2a$ (Δx)	RMS error
0.800	0.9806×10^{-1}
0.400	0.3674×10^{-1}
0.200	0.9642×10^{-2}
0.100	0.2456×10^{-2}
0.050	0.6174×10^{-3}
0.025	0.2193×10^{-3}

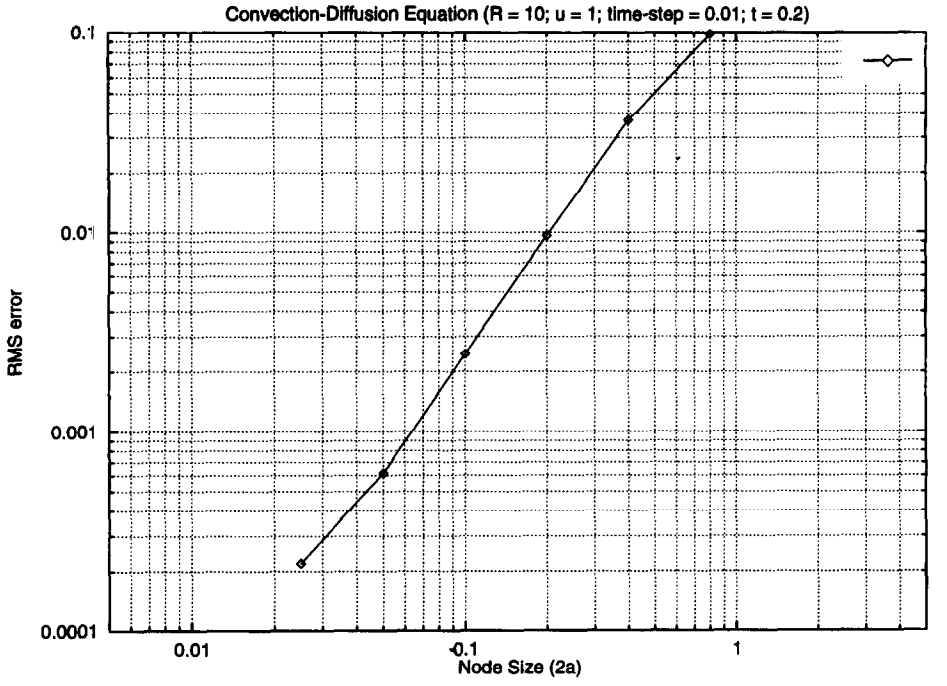

Fig. 3. RMS error in the solution of the convection–diffusion equation plotted versus node size $2a$.

dispersion adds numerical diffusion, as is evident in the solution. The CN-4PU solution also shows spurious oscillations before and after the propagating front.

To demonstrate the node interior reconstruction capability of the NIM, we solve the convection–diffusion equation for $R = 5$ with only 7 nodes over $-2 \leq x \leq 2$. The time-averaged solution at the six interior node surfaces is shown in Fig. 7. Corresponding exact solution and the NIM-based reconstructed solution are also shown. Although the error in the NIM reconstructed solution at node surfaces obviously does not change, the node reconstructed interior solution is definitely, in general, better than the solution obtained by connecting the neighboring node surface solutions by straight lines.

3.2. Example 2

The second problem solved using the method developed above has a time-dependent boundary condition. The domain of the problem is restricted to [0,2], and the initial and boundary conditions are

$$C(x,0) = 0$$

$$C(x = 0,t) = e^{-\lambda t}$$

Table 2. RMS error vs time step

2τ (Δt)	RMS error
0.64	0.6296×10^{-1}
0.48	0.4312×10^{-1}
0.32	0.2314×10^{-1}
0.24	0.1402×10^{-1}
0.16	0.6462×10^{-2}
0.08	0.1586×10^{-2}
0.04	0.4640×10^{-3}
0.02	0.2309×10^{-3}
0.01	0.1908×10^{-3}

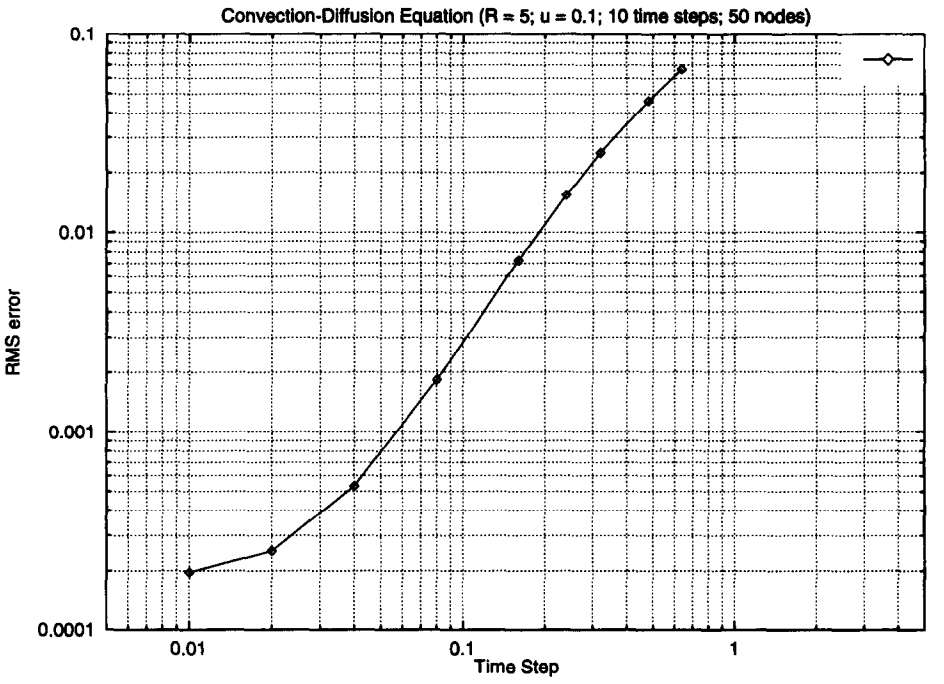

Fig. 4. RMS error in the solution of the convection–diffusion equation versus time step.

and

$$\frac{\partial C(x,t)}{\partial x} = 0 \text{ as } x \to \infty.$$

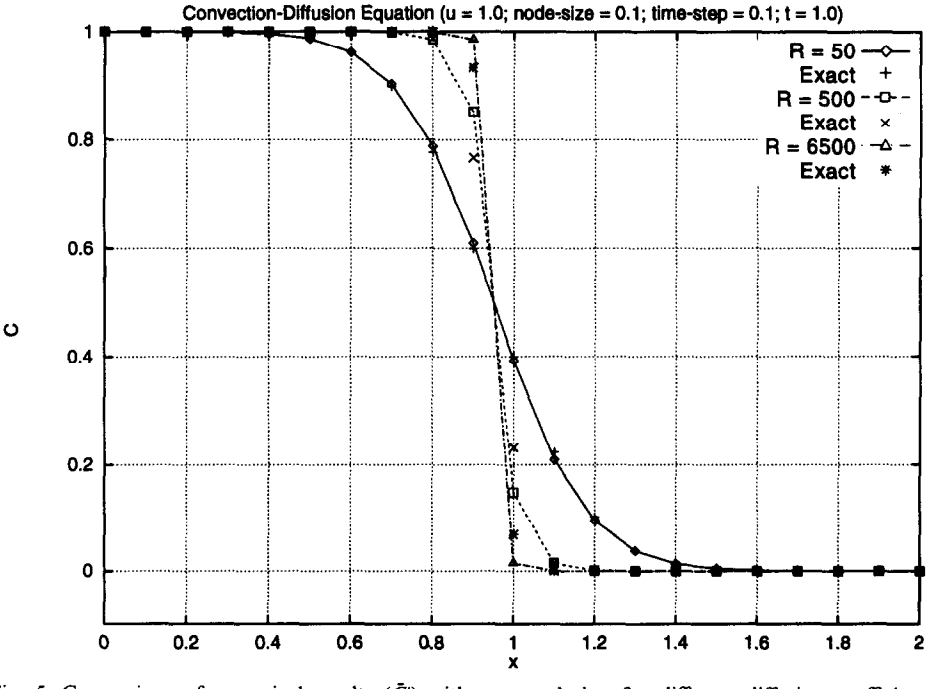

Fig. 5. Comparison of numerical results ($\tilde{C}'$) with exact solution for different diffusion coefficients ($D = 1/R$).

Table 3. Comparison between NIM and CN-4PU ($u = 1.0$, $\Delta x = 0.1$, $\Delta t = 0.1$)

R	Error in NIM	Error in CN-4PU
100	0.7326×10^{-2}	0.1554×10^{-1}
500	0.1944×10^{-1}	0.4728×10^{-1}
1000	0.2001×10^{-1}	0.5533×10^{-1}
2500	0.1663×10^{-1}	0.5724×10^{-1}
5000	0.1337×10^{-1}	0.5705×10^{-1}
6500	0.1217×10^{-1}	0.5699×10^{-1}

The concentration at the left boundary decreases exponentially in time. An exact solution of the above problem is [9, 20]

$$C(x,t) = (1/2)\,e^{-\lambda t}\left[\exp\left(\frac{(u-\alpha)xR}{2}\right) erfc\left(\left(\frac{x-\alpha t}{2}\right)\sqrt{\frac{R}{t}}\right)\right.$$
$$\left. + \exp\left(\frac{(u+\alpha)xR}{2}\right) erfc\left(\left(\frac{x+\alpha t}{2}\right)\sqrt{\frac{R}{t}}\right)\right] \quad (21)$$

where $\alpha \equiv (u^2 - 4\lambda/R)^{1/2}$. Since the analytical solution in space is for a fixed time t, and the numerical solution using the NIM is the concentration averaged over a time step, a quantitative comparison between them—especially for a large time step—should not be carried out. If necessary, one can numerically integrate the analytical solution for a fixed x, over a time step. Since we have

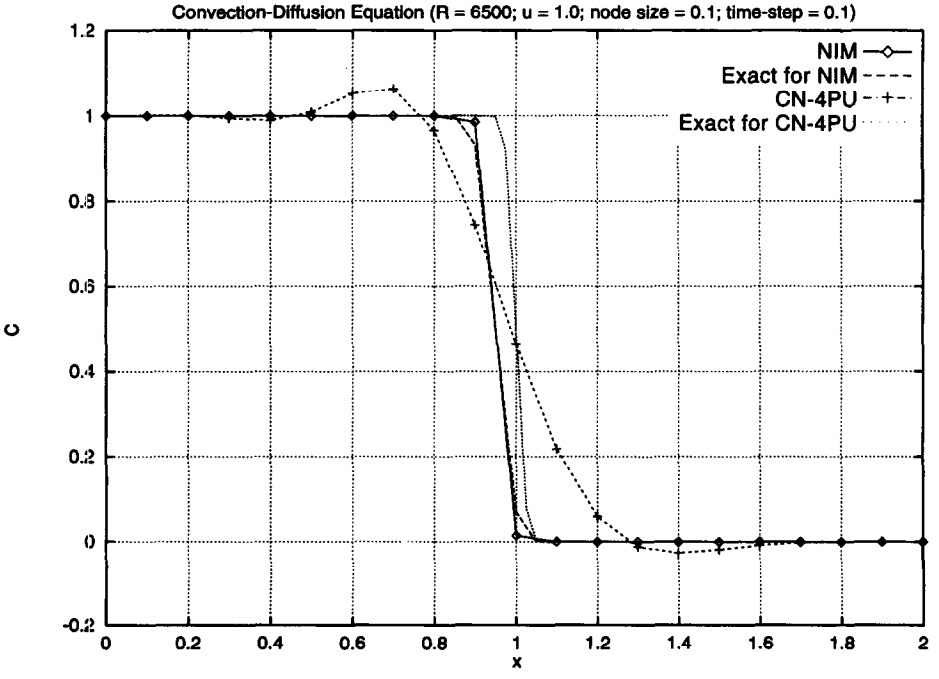

Fig. 6. A general comparison for the propagating concentration front problem among the exact solution, NIM, and CN-4PU for $Re = 6500$. Values plotted for CN-4PU scheme and the corresponding exact solution are at $t = 1.0$. Values plotted for NIM and its corresponding exact solution are the quantities averaged over the last time interval, $\bar{C}^{l}_{ij}$.

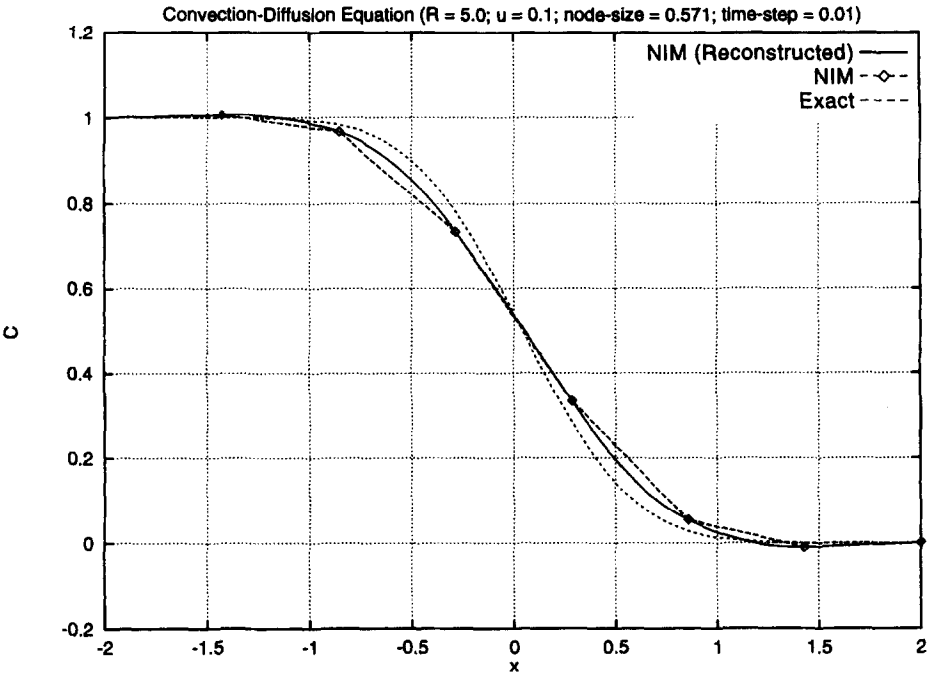

Fig. 7. A comparison of the seven-node solution ($\bar{C}'$) obtained using the NIM (point values) and the node interior reconstructed solution with the exact solution.

already demonstrated the numerical quantitative comparison in example one, it is not repeated here. Figure 8 shows the analytical solution at $t = 2$, 4 and 6, and the corresponding NIM solution. The solution at small time ($t = 2$) does show a small wiggle which disappears as t increases. Overall, the NIM, even for a problem with time-varying boundary conditions, performs quite well.

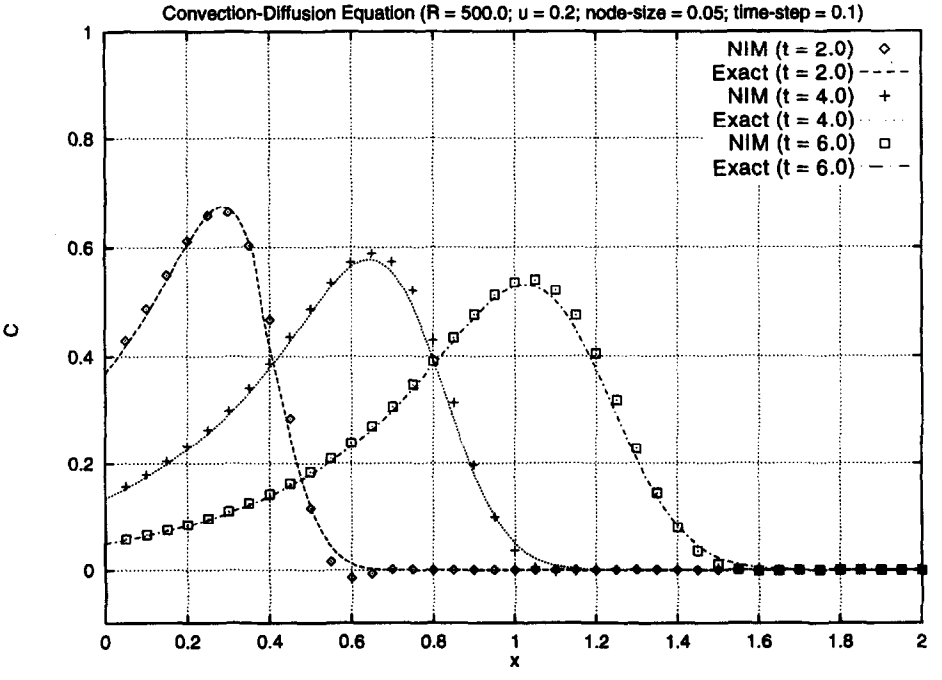

Fig. 8. Comparison of the time-averaged concentration ($\bar{C}'$) calculated using the NIM for the second numerical example (time-dependent boundary condition) with the corresponding exact solution.

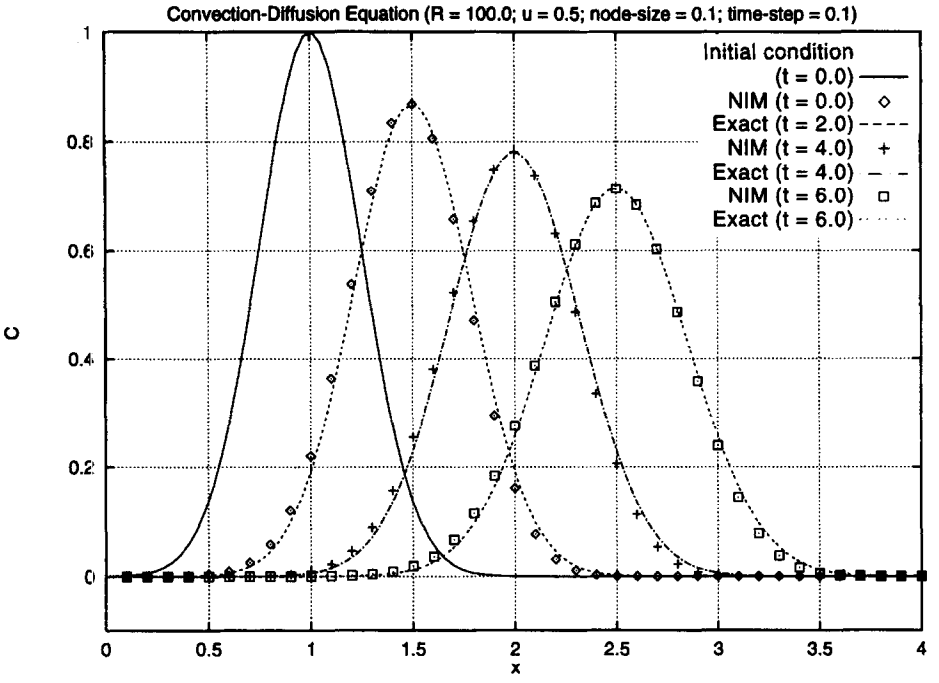

Fig. 9. Comparison of the time-averaged concentration ($\bar{C}'$) calculated using the NIM for the third numerical example (Gaussian hump) with the corresponding exact solution.

3.3. *Example* 3

Propagation and diffusion of a Gaussian hump in an infinite domain also has an exact analytical solution, and is often used to demonstrate the accuracy and efficiency of numerical techniques. The exact solution is [9, 21]

$$C(x,t) = \frac{\sigma_0}{\sigma} \exp\left[- \frac{(x - x_0 - ut)^2}{2\sigma^2} \right]$$

$$\sigma^2 = \sigma_0^2 + 2t/R \tag{22}$$

where the Gaussian hump with (initial) standard deviation σ_0 is initially located at $x = x_0$. The initial condition is, hence

$$C(x,0) = \exp\left[\frac{-(x - x_0)^2}{2\sigma_0^2} \right] \tag{23}$$

and for convenience we choose the boundary condition for the finite domain to be

$$C(x = x_l, t) = 0$$

$$\frac{\partial C(x = x_r, t)}{\partial x} = 0$$

where x_l and x_r are the left and right boundaries of the finite domain. We make sure that the spatial domain is large enough to mimic the infinite domain solution accurately.

The NIM solution and the exact solution at $t = 1$, 2, and 3 for $x_0 = 1$ and $\sigma_0 = 0.25$—which corresponds to a rather narrow hump—are shown in Fig. 9. The diffusion coefficient $D = 1/R = 0.01$ and velocity is 0.5. Clearly, the NIM captures the moving peak's magnitude and location very well.

4. DISCUSSION

The second-order nodal method described above for a one-dimensional time-dependent convection–diffusion equation has several unique characteristics. Most important of these, we

believe, is the inherent upwinding in the final scheme. Upwind schemes—when imposed somewhat arbitrarily based on flow direction—have been criticized, sometimes for good reasons [20, 21]. In the numerical scheme developed here it results automatically: while determining the concentration at node (i,j) the coefficients of the concentration in the left and right nodes (node $(i-1,j)$) and node $(i+1,j)$) automatically adjust based on both flow direction and diffusion coefficient. That is, the weight of the downstream node is zero only when there is no diffusion. When there is diffusion present, the weights are appropriately calculated to account for both convection and diffusion.

Stability of the NIM was studied numerically. The method is quite robust and does not lead to spurious oscillations even for very small diffusion coefficients (large Peclet numbers). The method was found to be stable for moderate to large Courant numbers (> 1), but showed beginning of oscillations at Courant number above 2.5. Results presented in Fig. 2(a,b), Fig. 5, and Fig. 6 are obtained with a Courant number of 1.

Although a similar analysis of the NIM for the time-dependent one-dimensional convection–diffusion equation has not been carried out, it was shown that the NIM for the two-dimensional steady-state convection–diffusion equation reduced to the nodal method for the pure-convection problem in the limit of large *Pe*; and it reduced to the NIM for the pure-diffusion problem in the limit of zero *Pe* [16]. A similar trend is seen here for the NIM developed for the time-dependent problem which shows higher RMS errors for intermediate values of *Pe* than for very small or very large values. Solution of Examples 2 and 3 using the NIM showed that the nodal method does exhibit some small systematic errors.

The node interior reconstruction of the solution—that is actually carried out after the node surface values have been solved—indicates that the nodal method can yield accurate node interior solution; more accurate than the solution obtained by connecting the node surface values by straight lines.

Application of the method to three examples shows that the second-order method is capable of accurately solving difficult problems with steep concentration gradients. Extension of this method to adaptive grids can further improve its capability to solve difficult problems with even fewer nodes.

5. SUMMARY

A nodal integral method has been developed to solve the convection–diffusion equation. Space as well as time coordinates are treated using the nodal approach, leading to a method that is second order both in space and time. The final scheme is also characterized by inherent upwinding. Numerical examples show that the method can be used to solve rather difficult problems accurately (steep concentration gradients, and very large and small Peclet numbers) without introducing artificial viscosity, and does not show signs of numerical dissipation or dispersion.

Acknowledgement—This work was supported by NASA under grant number NAGW/3021.

REFERENCES

1. Fletcher, C. A. J., *Computational Techniques for Fluid Dynamics I*. Springer, New York, 1988.
2. Yanenko, N. N., *The Method of Fractional Steps*. Springer, Berlin, 1971.
3. Gourlay, A. R. and Morris, J. L., A multi-step formulation of the optimized Lax–Wendroff method for non-linear hyperbolic systems in two space variables. *Math. Comp.*, 1968, **22,** 715–720.
4. Muralidhar, K., Verghese, M. and Pillai, K. M., Application of an operator-splitting algorithm for advection–diffusion problems. *Numer. Heat Transfer A*, 1993, **23,** 99–113.
5. Perot, J. B., An analysis of the fractional step method. *J. Comput. Phy.*, 1993, **108,** 51–58.
6. Xin, X. K. and Wong, Y. S., Eulerian–Lagrangian splitting methods for convection dominated equations. *Fluid Dynamic Res.*, 1989, **5,** 13–27.
7. Le Veque, R. J., Intermediate boundary conditions for time-split methods applied to hyperbolic partial differential equations. *Math. Comp.*, 1986, **47, 175,** 37–54.
8. Aiyesimoju, K. O. and Sobey, R. J., Process splitting of boundary conditions for the advection–diffusion equation. *Int. J. Numer. Methods Fluids*, 1989, **9,** 235–244.
9. Khan, L. A. and Liu, P. L.-F., Intermediate Drichlet boundary conditions for operator splitting algorithms for the advection–diffusion equation. *Computers & Fluids*, 1995, **24,** 447–458.
10. Horak, W. C. and Dorning, J. J., A nodal coarse-mesh method for the efficient numerical solution of laminar flow problems. *J. Comp. Phys.*, 1985, **59,** 405–440.
11. Lawrence, R. D. and Dorning, J. J., A nodal Green's function method for multidimensional neutron diffusion calculations. *Nucl. Sci. Engng*, 1980, **76,** 218–231.

12. Azmy, Y. Y., A nodal integral method for the numerical solution of incompressible fluid flow problems. Master's thesis, University of Illinois, 1982.
13. Azmy, Y. Y. and Dorning, J. J., A nodal integral approach to the numerical solution of partial differential equations. In *Advances in Reactor Computations*, Volume II, pp. 893–909. American Nuclear Society, LaGrange Park, IL, 1983.
14. Wilson, G. L., Rydin, R. A. and Azmy, Y. Y., Time-dependent nodal integral method for the investigation of bifurcation and nonlinear phenomena in fluid flow and natural convection. *Nucl. Sci. Engng*, 1988, **100**, 414–425.
15. Elnawawy, O. A., Valocchi, A. J. and Ougouag, A. M., The cell analytical-numerical method for solution of the advection–dispersion equation: two-dimensional problems. *Water Resources Res.*, 1990, **26, 11**, 2705–2716.
16. Michael, E. P. E., Dorning, J. J., Gelbard, E. M. and Rizwan-uddin., A nodal integral method for the convection-diffusion heat equation. *Trans. Am. Nucl. Soc.*, 1993, **69**, 239–241.
17. Michael, E. P. E., Dorning, J. J. and Rizwan-uddin., A third-order nodal integral method for the convection–diffusion equation. *Trans. Am. Nucl. Soc.*, 1994, **71**, 195–197.
18. Decker, W. J., A block iterative nodal-integral method for fluid dynamics problems. M.S. thesis, University of Virginia, 1995.
19. Rizwan-uddin., An improved coarse-mesh nodal integral method for partial differential equations. *Numerical Methods for Partial Differential Equations*, in press.
20. van Genuchten, M. Th., Analytical solutions for chemical transport with simultaneous adsorption. Zero-order production and first-order decay. *J. Hydrology*, 1981, **49**, 213–233.
21. Gresho, P. M. and Lee, R. L., Don't suppress the wiggles—they're telling you something!. *Computers & Fluids*, 1981, **9**, 223–253.